T. Magn. Soc. Jpn. (Special Issues)., **1**, 26-29 (2017)

<Paper>

Size dependence of magnetic properties for $L1_0$-MnGa circular dots

H. Makuta, Y. Takahashi, T. Shima, and M. Doi

Graduate School of Engineering, Tohoku Gakuin University, *1-13-1 Chuo, Tagajo-shi, Miyagi 985-8537, Japan*

$L1_0$-MnGa circular dot arrays have been microfabricated from continuous films. The thin films were prepared using an alternate deposition method with a magnetron sputtering system. Improvement of degree of long-range order (S) and saturation magnetization (M_s), for the $L1_0$-MnGa thin film was confirmed when repetition number (n) was increased to 10. The thin film with n = 10 exhibited M_s = 439 kA/m and K_u = 1.1 MJ/m^3. The film with n = 10 was microfabricated into circular dot arrays by electron beam (EB) lithography and Ar ion milling. The critical single-domain size was determined to be 140 nm$^\varphi$ by observation of magnetic domain using a magnetic force microscope, and the exchange stiffness constant ($A_{const.}$) was then estimated to be 1.1 × 10^{-11} J/m from the critical single-domain size.

Keywords: $L1_0$-MnGa thin film, circular dot arrays, microfabrication, critical single-domain size, exchange stiffness constant

1. Introduction

$L1_0$-MnGa alloy attracts much attention as one of material exhibiting high uniaxial crystalline magnet anisotropy without including rare earth elements or noble metals. The $L1_0$ structure is corresponding to γ_1 and γ_2 -phase in the Mn-Ga binary phase diagram[1], it is thermodynamically stable in range of approximately 64 ~ 67 (γ_1-phase) and 58 ~ 61 (γ_2-phase) at. % Mn. In thin film case, saturation magnetization $M_s \approx$ 600 kA/m and uniaxial magnetic anisotropy $K_u \approx 1.5 \times 10^6$ J/m^3 have been reported in $Mn_{54}Ga_{46}$ (at. %) sputtered thin film[2]. Such high K_u of $L1_0$-MnGa above 1 MJ/m is satisfying requirement to maintain the magnetization direction even in a nanoscale magnet. Therefore, a lot of studies about the $L1_0$-MnGa and the application such as the thin films on various substrates[3)-6)], microparticles with nanocrystal[7)], spintronics devises[8)-9)], and a bit patterned media[10)] have been performed. However, there are few reports about magnetic properties for the $L1_0$-MnGa in nanoscale. Understanding of nanoscale magnetic properties should be required for the design guidelines for the various applications.

In this study, $L1_0$-MnGa circular dot arrays have been microfabricated from the thin films. A relation between the magnetic properties and the diameter of the dots has also been investigated. The critical single-domain size was determined by observation of magnetic domain using a magnetic force microscope; exchange stiffness constant ($A_{const.}$) was then estimated from the critical single-domain size.

2. Experimental procedure

The $L1_0$-MnGa thin films were prepared by alternate deposition method with radio-frequency magnetron sputtering system. Base pressure of the deposition chamber was less than 1 × 10^{-5} Pa. [Mn/MnGa]$_n$ (n: repetition number) multilayers were deposited on a Cr (5 nm) buffered MgO (001) single crystal substrate. The stacks were then capped by a Cr layer (10 nm). n was varied as followed: n = 5, 10, and 15, whereas total thickness of the [Mn/MnGa]$_n$ multilayer was fixed at 20 nm. The Cr buffer layer was deposited at room temperature (R.T.), and annealed at 700ºC for 30 min. The [Mn/MnGa]$_n$ multilayers were deposited at 100ºC by using a Mn and $Mn_{40}Ga_{60}$ alloy target for the Mn and MnGa layer respectively, and then post-annealing were applied at 400ºC for 60 min to promote crystallization $L1_0$ ordering of the [Mn/MnGa]$_n$ multilayers. Composition of the $L1_0$-MnGa film can be controlled by change of thickness ratio for the Mn and MnGa layer in the multilayer. The composition was fixed at $Mn_{58}Ga_{42}$ (at. %), in this case thicknesses of the Mn and MnGa layer were approximately [Mn (0.97 nm)/MnGa (3.0 nm)]$_5$, [Mn (0.49 nm)/MnGa (1.5 nm)]$_{10}$, and [Mn (0.32 nm)/MnGa (1.0 nm)]$_{15}$. The $L1_0$-MnGa dots were microfabricated from the continuous films through the use of electron beam (EB) lithography with a negative-type EB resist and Ar ion milling. After the milling process, the dots were capped by an Au layer (5 nm) without exposure to atmosphere to protect side of the dots from oxidation. Diameter of the dot (D) was reduced from 1000 nm$^\varphi$ to 140 nm$^\varphi$. The crystalline structures of the thin films were identified by 2θ-θ scans of x-ray diffraction (XRD) with Cu-$K\alpha$ radiation. The magnetic properties for the films were measured with a super conducting quantum interference device (SQUID) magnetometer. The shapes of the dots were observed using an atomic force microscope (AFM). The magnetic properties for the dots were characterized using the magneto-optical Kerr effect (μ-MOKE) measurement system with the polar configuration. Magnetic domain structures were observed using a magnetic force microscope (MFM). All the measurements were performed at R.T..

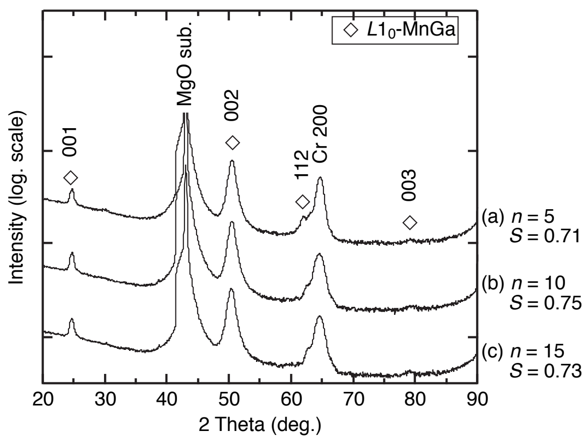

Fig. 1 XRD patterns for $L1_0$-MnGa thin films with repetition number (n) = (a) 5, (b) 10, and (c) 15.

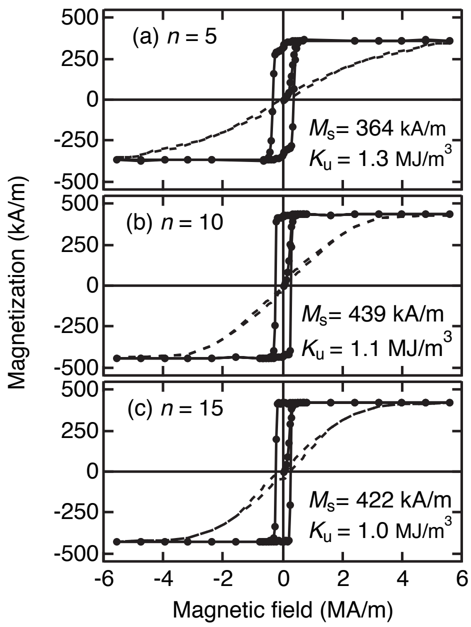

Fig. 2 Magnetization curves for $L1_0$-MnGa thin films with repetition number (n) = (a) 5, (b) 10, and (c) 15. Solid circles and dashed lines denote out-of-plane and in-plane curves respectively.

3. Results and discussion

First, in order to find optimum n of the $[Mn/MnGa]_n$ multilayer, investigate the effect of n on crystalline structure and magnetic properties for the thin film. Fig. 1 shows XRD patterns for the $L1_0$-MnGa films with $n = 5$ (a), 10 (b), and 15 (c). Fundamental (002) peaks and superlattice (001), (003) peaks of $L1_0$-MnGa were observed in $n = 5 \sim 15$. It indicating that the $L1_0$-MnGa films were successfully obtained from the $[Mn/MnGa]_n$ multilayer after post-annealing. A (112) peak was also clearly observed in $n = 5$. It implies incomplete orientation along [001] direction (i.e., easy axis of magnetization) of the MnGa layer. In case of $n = 10$ and 15, the (112) peak intensity was reduced compared to the film with $n = 5$, indicating improve of [001] orientation of the MnGa layer with n increase. The degree of long-range order (S) was estimated from following Eq. (1):

$$S = \sqrt{[I_{(001)}/I_{(002)}]_{meas.}} / \sqrt{[I_{(001)}/I_{(002)}]_{calc.}}, \quad (1)$$

where $I_{(001)}$ and $I_{(002)}$ are integrated intensity of (001) and (002) peaks and $[I_{(001)}/I_{(002)}]_{meas.}$ and $[I_{(001)}/I_{(002)}]_{calc.}$ are the measured and calculated peak intensity ratio, respectively. When n was increased to 10 from 5, S was slightly increased to 0.75 from 0.71. It can be interpreted as a result that increase of interfaces between the Mn and MnGa layers in the multilayer allowed easy crystallization and $L1_0$ ordering.

Fig. 2 shows magnetization curves for the $L1_0$-MnGa films with $n = 5$ (a), 10 (b), and 15 (c). Solid circles and dashed lines denote the out-of-plane and in-plane curves respectively. K_u was estimated from estimated Eq. (2):

$$K_u = \mu_0 M_s \times H_k/2 + \mu_0 M_s^2/2, \quad (2)$$

where μ_0 is space permeability, and H_k is anisotropy field. $\mu_0 M_s^2/2$ is correction of the demagnetizing energy. H_k of the films were estimated to be 5.2 MA/m for $n = 5$, 3.5 MA/m for $n = 10$ and 15. M_s was increased to $M_s = 439$ kA/m from 364 kA/m, K_u was decreased to 1.1 MJ/m^3 from 1.3 MJ/m^3 when n was increased to 10 from 5. In case of $n = 15$, remarkable changes in M_s and K_u were not observed.

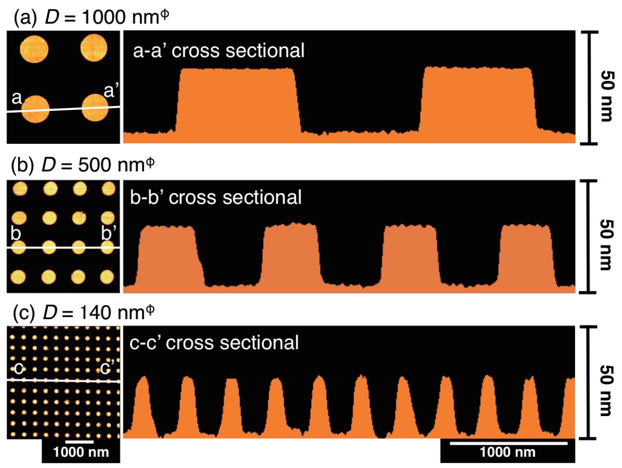

Fig. 3 AFM plane view and cross-sectional images for $L1_0$-MnGa dots with D = (a) 1000 nm$^\varphi$, (b) 500 nm$^\varphi$, and (c) 140 nm$^\varphi$.

The $L1_0$-MnGa film of $n = 10$ with maximum S and M_s was microfabricated into the $L1_0$-MnGa circular dot arrays. Fig. 3 shows representative AFM plane view and cross-sectional images for the $L1_0$-MnGa dots with D = 1000 nm$^\varphi$ (a), 500 nm$^\varphi$ (b), and 140 nm$^\varphi$ (c). The dots with well-defined circular shapes were observed for each D in the AFM images.

Fig. 4 shows MOKE curves for the as-deposited $L1_0$-MnGa continuous film (a) and the as-patterned dots with D = 1000 nm$^\varphi$ (b), 700 nm$^\varphi$ (c), 500 nm$^\varphi$ (d), 300 nm$^\varphi$

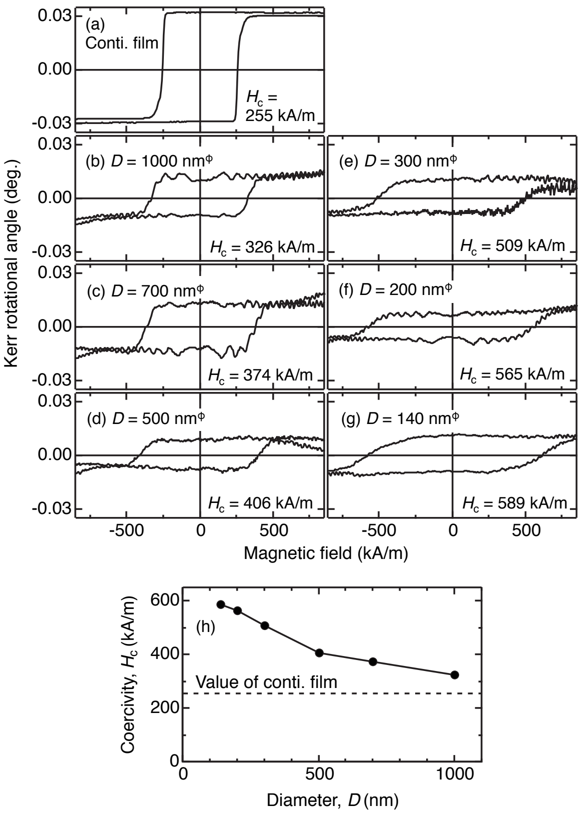

Fig. 4 MOKE curves for $L1_0$-MnGa (a) continuous film and dots with D = (b) 1000 nmφ, (c) 700 nmφ, (d) 500 nmφ, (e) 300 nmφ, (f) 200 nmφ, and (g) 140 nmφ. (h) Coercivity (H_c) as a function of diameter (D) for the dots.

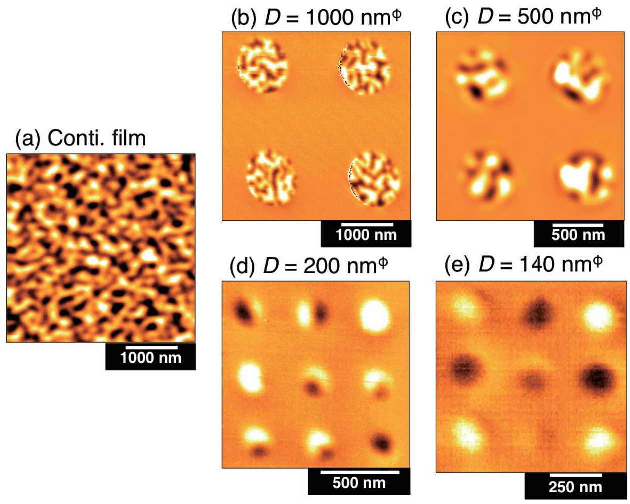

Fig. 5 MFM images of $L1_0$-MnGa (a) continuous film and dots with D = (b) 1000 nmφ, (c) 500 nmφ, (d) 200 nmφ, and (e) 140 nmφ in initial state. Bright and dark contrast denotes the upward and downward magnetization state, respectively.

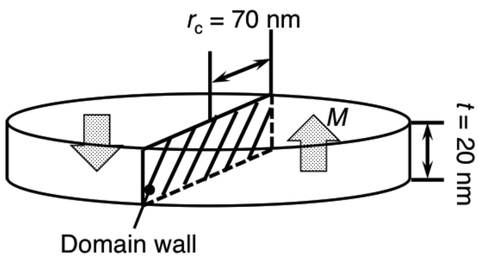

Fig. 6 Schematic illustration of a circular dot with double-domain structure.

(e), 200 nmφ (f), and 140 nmφ (g); coercivity (H_c) as a function of D for the dots is shown in (h). When the continuous film with H_c = 255 kA/m was microfabricated into the dots with D = 1000 nmφ, it exhibits H_c = 326 kA/m. H_c was more increased with decrease of D, H_c = 589 kA/m was confirmed in D = 140 nmφ.

In order to determine the critical single-domain size of the $L1_0$-MnGa thin film, observation of the magnetic domain by using a MFM was carried out. Fig. 5 shows MFM images of the as-deposited $L1_0$-MnGa continuous film (a) and the as-patterned dots which were magnetically initial state with D = 1000 nmφ (b), 500 nmφ (c), 200 nmφ (d), and 140 nmφ (e). The bright and dark contrast denotes the upward and downward magnetization state respectively. Multiple-domain structure was observed for the continuous film and the dots with D = 300 nmφ whereas few dots with single-domain structure was observed among the dots with double-domain structure in D = 200 nmφ. When D was decreased to 140 nmφ, single-domain structure was observed for most of the dots. It suggests that critical single-domain size of the $L1_0$-MnGa dot is D = 140 nmφ.

$A_{const.}$ of the $L1_0$-MnGa dot was estimated using the critical single-domain size. Here, domain wall energy and magnetostatic energy in a dot with critical diameter is discussed. Fig. 6 is a schematic illustration of a circular dot with double-domain structure. Domain wall energy of the dot (γ) is given by

$$\gamma = 2 r_c t \pi \sqrt{A_{const.} K_u}, \qquad (3)$$

where r_c is the critical single-domain radius and t is thickness of the dot. On the other hand, if the dot has single-domain structure, magnetostatic energy of the dot (U_m) is given by

$$U_m = \mu_0 N \pi r_c^2 t M_s^2/2, \qquad (4)$$

where N is demagnetizing factor of the out-of-plane direction. In the critical case,

$$\gamma = U_m. \qquad (5)$$

Therefor, the following Eq. (6) is satisfied:

$$2 r_c t \pi \sqrt{A_{const.} K_u} = \mu_0 N \pi r_c^2 t M_s^2/2. \qquad (6)$$

From Eq. (6), $A_{const.}$ is described as

$$A_{const.} = r_c^2 N^2 \mu_0^2 M_s^4 / 16 K_u. \qquad (7)$$

Using the r_c = 70 nm, N = 0.81, M_s = 439 kA/m, and K_u = 1.1 MJ/m^3, $A_{const.}$ is estimated to be 1.1 × 10^{-11} J/m. Magnetic properties for the representative ferromagnetic materials including the $L1_0$-MnGa is summarized in Table 1. The $A_{const.}$ of the $L1_0$-MnGa is comparable to that of the other listed materials.

Table 1 Magnetic properties for the representative ferromagnetic materials.

Material	$\mu_0 M_s$ (T)	K_u (J/m^3)	$2r_c$ (nm)	$A_{const.}$ (J/m)	Ref.
Fe	2.15	$\approx 4.2 \times 10^4$	12	2.0×10^{-11}	11)
Co	1.80	$\approx 5.3 \times 10^5$	70	1.3×10^{-11}	11)
$L1_0$-FePt	1.45	$\approx 6.6 \times 10^6$	340	1.6×10^{-11}	12) - 14)
Nd-Fe-B	1.60	$\approx 4.5 \times 10^6$	210	0.8×10^{-11}	15)
$L1_0$-MnGa	0.55	$\approx 1.1 \times 10^6$	140	1.1×10^{-11}	—

As presented above, H_c, critical single-domain size, and $A_{const.}$ of the $L1_0$-MnGa dots were demonstrated. However, it must be note that the dots were as-patterned; consequently, deterioration of the magnetic properties due to the damage of the dots during the milling process must be considered. Post-annealing of the dots and investigation of magnetic properties for the dots are should be required.

4. Summary

In this study, $L1_0$-MnGa circular dot arrays have been microfabricated from the thin films. A relation between the magnetic properties and the diameter of the dots has also been investigated. The $L1_0$-MnGa thin films were prepared by alternate deposition method. Improvement of S, and M_s for the $L1_0$-MnGa thin film was confirmed when n of the [Mn/MnGa]$_n$ multilayer before post-annealing was increased to 10 from 5. The film with n = 10 exhibits M_s = 439 kA/m and K_u = 1.1 MJ/m^3. The film with n = 10 was microfabricated into the circular dot arrays. The critical single-domain size was determined to be 140 nm$^\varphi$ by observation of magnetic domain using a magnetic force microscope, and $A_{const.}$ was then estimated to be 1.1×10^{-11} J/m from the critical single-domain size.

Acknowledgments

This study was performed at the Hi-tech Research Center of Tohoku Gakuin University, and supported by "Collaborative Research Based on Industrial Demand" program from Japan Science and Technology Agency.

References

1) K. Minakuchi, R. Y. Uematsu, K. Ishida, and, R. Kainuma: *J. Alloy. Compod.*, **537**, 332 (2012).
2) S. Mizukami, T. Kubota, F. Wu, X. Zhang, and T. Miyazaki: *Phys. Rev. B*, **85**, 014416 (2012).
3) K. Wang, A. Chinchore, W. Lin, D. C. Ingram, A. R. Smith, A. J. Hauser, and F. Yang: *J. Cryst. Growth*, **311**, 2265 (2009).
4) W. Feng, D. V. Thiet, D. D. Dung, Y. Shin, and S. Cho: *J. Appl. Phys.*, **108**, 113903 (2010).
5) C. L. Zha, R. K. Dumas, J. W. Lau, S. M. Mohseni, S. R. Sani, I. V. Golosovsky, A. F. Monsen, J. Nogues, and J. Akerman: *J. Appl. Phys.*, **110**, 093902 (2011).
6) K. Wang, E. Lu, J. W. Knepper, F. Yang, and A. R. Smith: *Appl. Phys. Lett.*, **98**, 162507 (2011).
7) B. Z. Cui, M. Marinescu, and J. F. Liu: *IEEE Trans. Magn.*, **49**, 3322 (2013).
8) Q. L. Ma, T. Kubota, S. Mizukami, X. M. Zhang, H. Naganuma, M. Oogane, Y. Ando, and T. Miyazaki: *Appl. Phys. Lett.*, **101**, 032402 (2012).
9) Q. L. Ma, S. Mizukami, T. Kubota, X. M. Zhang, Y. Ando, and T. Miyazaki: *Phys. Rev. Lett.*, **112**, 157202 (2014).
10) D. Oshima, T. Kato, S. Iwata, and S. Tsunashima: *IEEE Trans. Magn.*, **49**, 3608 (2013).
11) Y. Iwama: Jiki Kougaku Kouza 3 Koshitsu Jisei Zairyo (in Japanese), p. 18 - 20 (Maruzen, Tokyo, 1976).
12) O. A. Ovanov, L. V. Solima, V. A. Demashina, and L. M. Magat: *Phys. Met. Metalloger.*, **35**, 81 (1973).
13) T. Klemmer, D. Hoydick, H. Okumura, B. Zhang, and W. A. Soffa: *Scr. Metall. et Materi.*, **33**, 1793 (1995).
14) D. Hinzke, N. Kazantseva, U. Nowak, O. N. Mryasov, P. Asselin, and R. W. Chantrell: *Phys. Rev. B*, **77**, 094407 (2008).
15) K. Hono, S. Hirosawa: Progress of Fundamentals and Developments of Novel Nd-Fe-based Permanent Magnets Free from Dy, p. 18, 239 (CMC Shuppan, Tokyo, 2015).

Received Oct. 11, 2016; Accepted Dec. 13, 2016